land

MDPI

Article

Ecosystem Resilience Trends and Its Influencing Factors in China's Three-River Headwater Region: A Comprehensive Analysis Using CSD Indicators (1982–2023)

Zishan Wang [1], Wenli Huang [2,*] and Xiaobin Guan [2]

[1] College of Life Sciences, Wuhan University, Wuhan 430072, China; zishanwang@whu.edu.cn
[2] School of Resource and Environmental Sciences, Wuhan University, Wuhan 430079, China; guanxb@whu.edu.cn
* Correspondence: wenli.huang@whu.edu.cn

Abstract: Ecosystem resilience, the ability of an ecosystem to recover from disturbances, is a critical indicator of environmental health and stability, particularly under the impacts of climate change and anthropogenic pressures. This study focuses on the Three-River Headwater Region (TRHR), a critical ecological area for East and Southeast Asia, often referred to as the "Water Tower of China". We used the Normalized Difference Vegetation Index (NDVI) as a proxy for vegetation growth and productivity and calculated Critical Slowing Down (CSD) indicators to assess the spatiotemporal dynamics of grassland ecosystem resilience in the TRHR from 1984 to 2021. Our research revealed a sustained improvement in ecosystem resilience in the TRHR starting in the late 1990s, with a reversal in this trend observed after 2011. Spatially, ecosystem resilience was higher in areas with greater precipitation and higher vegetation productivity. Temporally, changes in grazing intensity were most strongly correlated with resilience dynamics, with explanatory power far exceeding that of NDVI, temperature, and precipitation. Our study underscores the importance of incorporating ecosystem resilience into assessments of ecosystem function changes and the effectiveness of ecological conservation measures, providing valuable insights for similar research in other regions of the world.

Keywords: ecosystem resilience; alpine meadow; Three-River Headwater Region; critical slowing down; ecological management; tipping point; grazing; NDVI

Citation: Wang, Z.; Huang, W.; Guan, X. Ecosystem Resilience Trends and Its Influencing Factors in China's Three-River Headwater Region: A Comprehensive Analysis Using CSD Indicators (1982–2023). *Land* **2024**, *13*, 1224. https://doi.org/10.3390/land13081224

Academic Editors: Matteo Convertino and Jie Li

Received: 2 July 2024
Revised: 2 August 2024
Accepted: 3 August 2024
Published: 7 August 2024

1. Introduction

The Three-River Headwater Region (TRHR), known as the "Water Tower of China" [1], serves as the source of the Yangtze, Yellow, and Lantsang (Mekong) Rivers and plays a crucial role in water conservation, providing substantial ecological services to East and Southeast Asia and ensuring ecological security [2–4]. It is also one of the highest-altitude regions worldwide with the richest biodiversity, acting as a refuge for rare species [5]. As a river headwater area, its vegetation cover is vital for erosion control, flood mitigation, and water supply [6]. However, due to the TRHR's fragile ecological environment [7,8]; climate change; and social, economic, cultural, and policy influences leading to dramatic shifts in grazing intensity over recent decades [9], widespread and persistent grassland degradation has been observed since the mid-1970s, with desertification issues also present in semi-arid and arid areas [10]. These ecological risks have drawn widespread attention. Consequently, the Chinese government established the TRH reserve in 2000, injecting substantial funding and initiating large-scale ecological migration to protect the ecological environment of the TRHR [5]. Thus, the ecological environment of the TRHR is a typical area affected by both climate change and human activities, particularly the Kobresia meadows [11], the most widespread vegetation type in the region and the primary fodder type for livestock on the Qinghai-Tibetan Plateau, making it a focal area for grassland degradation [12]. Therefore, a

comprehensive analysis of the impact of climate change and human activities on vegetation in the TRHR is particularly crucial today.

Ecosystem resilience refers to the ability of an ecosystem to return to its original state after a disturbance or the rate at which it can do so, serving as a crucial indicator for assessing ecosystem health and stability, especially under uncertain future climate events [13–16]. With the intensification of global climate change and human activities, research on ecosystem resilience has increasingly gained attention. Numerous studies utilizing satellite remote sensing and ground observation data have demonstrated that since the establishment of the conservation area, vegetation productivity in the Three-River Headwater Region has significantly improved, enhancing ecosystem service functions [4,8,17]. For instance, the study by Zhai et al. (2020) [17] analyzing long-term NDVI data series showed a continuous increase in vegetation cover and biomass since 1998, particularly in alpine meadow and steppe ecosystems, closely associated with regional climate warming and management improvements. However, these studies primarily focused on changes in vegetation productivity, with few addressing the assessment of ecosystem resilience. To date, almost no research has evaluated the changes in ecological quality of the Three-River Headwater Region from the perspective of ecosystem resilience, which limits our comprehensive understanding of the region's ecosystem recovery and conservation effectiveness.

This study aims to fill this research gap by analyzing the changes in ecosystem resilience in the Three-River Headwater Region from 1984 to 2021, assessing the improvements in ecological quality since the establishment of the conservation area. To evaluate the vegetation growth condition of the ecosystem, we employed the Normalized Difference Vegetation Index (NDVI) as a proxy indicator. Vegetation productivity is a vital aspect of ecosystem function, and the NDVI is a widely used index in remote sensing research to estimate vegetation growth conditions and coverage. In grassland ecosystems in particular, which lack complex canopy structures and have lower biomass compared to forest ecosystems, the growth condition of grasslands can be more accurately reflected by satellite remote sensing data [18]. Therefore, the NDVI has been extensively used to estimate the vegetation status of grassland ecosystems [19–21], providing a reliable indicator of ecosystem productivity for our study.

We further adopted Critical Slowing Down (CSD) indicators as proxy variables for ecosystem resilience, constructing a dynamic model to characterize ecosystem resilience. The CSD approach is based on the principle that as an ecosystem approaches a critical threshold, its recovery rate from disturbances decreases and it exhibits greater fluctuations, which manifest as increased first-order time autocorrelation (AR(1)) and variance in growth conditions [22]. As a direct and quantitative modeling method, it has been widely used in recent years for evaluating ecosystem resilience. For example, Boulton et al. (2022) first pointed out that the Amazon rainforest experienced a tipping point in resilience in the early 2000s, providing evidence that the stability of the Amazon is under threat [23]. Global-scale analyses indicate that, in the long term, resilience has generally increased in tropical regions but decreased in high-latitude regions since the early 1990s [24]. Despite significant spatial heterogeneity, a tipping point in ecosystem resilience was widely observed globally in the early 2000s, especially in equatorial rainforest areas, which supported Boulton's findings, and the validation of different datasets mitigated concerns about data quality [24,25]. Focusing on smaller, specific study areas, Wu et al. (2023) analyzed changes in the resilience of grassland in Mongolia and Inner Mongolia since 2000, highlighting the significant impact of human activities [26]. However, there is still a lack of understanding regarding the dynamics and drivers of resilience in alpine grassland ecosystems, which is critical due to their unique ecological characteristics and vulnerability to climate change.

Therefore, by assessing the dynamics and driving factors of the ecosystem resilience of the TRHR, we aim to provide a scientific basis for the ecological restoration and sustainable management of this region, while also offering references for conservation and restoration efforts of similar ecosystems globally.

2. Materials and Methods

2.1. Study Area

The Three-River Headwater Region (TRHR) is located in the hinterland of the Qinghai-Tibetan Plateau (QTP), characterized by mountainous terrain and a dense river network, with altitudes ranging from 2700 m to 6600 m [27]. It features a plateau continental climate with low average annual temperatures, resulting in extensive permanently frozen ground. Precipitation increases from the northwest to the southeast, transitioning from semi-arid to semi-humid zones [4,28]. Our study area was defined according to the boundaries of the TRHR as published by the National Tibetan Plateau Data Center in 2018 [29], spanning longitudes from 89.40 E to 102.45 E and latitudes from 31.55 N to 37.10 N, covering a total area of 382,410 km^2 (Figure 1). From 1982 to 2018, the average annual temperature for the years 1982–2018 was 2.4 °C, gradually increasing with decreasing altitude (from −8.3 °C to 14.2 °C); the average annual precipitation was 589.3 mm, ranging from less than 50 mm to more than 1000 mm, although 86% of the area received annual precipitation between 200 and 800 mm [30–37]. The region's vegetation primarily consists of alpine steppes and meadows, which account for nearly 80% of the area's vegetation cover (Figure 1) [11]. The detailed physical characteristics of the Three-River Headwaters Region are shown in Table 1 (Table 1).

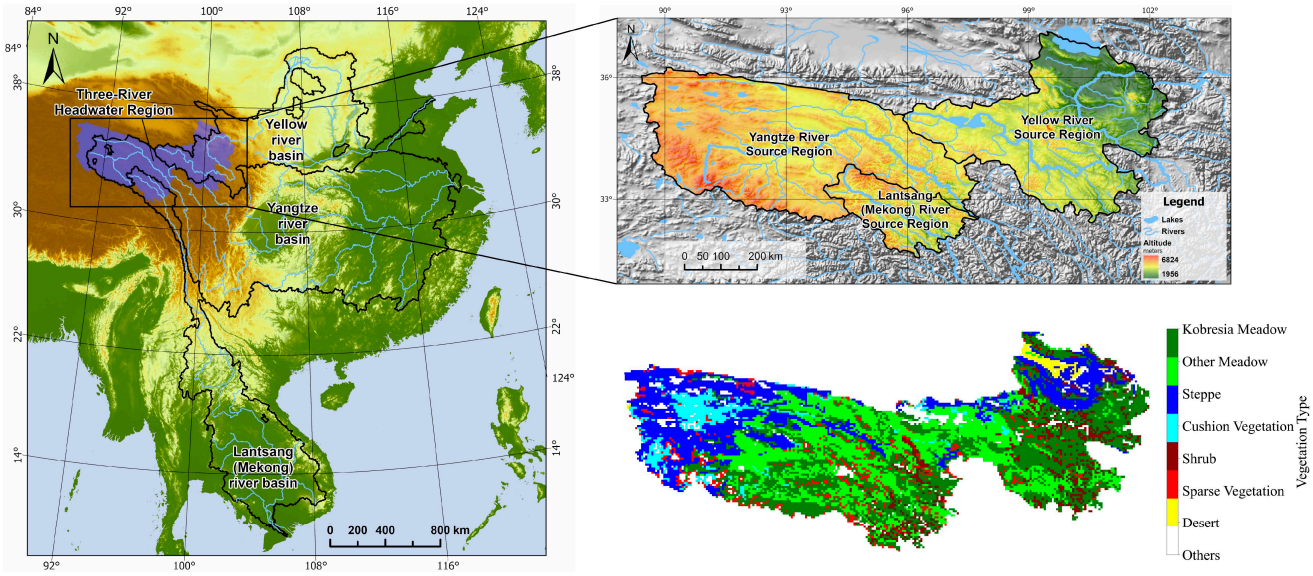

Figure 1. Location, terrain, and vegetation types of the study area.

Table 1. Physical characteristics of the three subregions of the TRHR.

Subregions	Mean Temperature	Mean Precipitation	Average Elevation	Dominant Vegetation Type
Yangtze River Source Region	1.68 °C	539.8 mm/year	4807.7 m	Alpine steppe
Yellow River Source Region	3.89 °C	617.4 mm/year	4035.4 m	Alpine meadow
Lantsang River Source Region	2.93 °C	717.7 mm/year	4603.3 m	Alpine meadow

In the 21st century, due to relevant national policies, 88% of the area has been prohibited or restricted from development, with cropland and built-up land accounting for only 1.2% [38]. Therefore, land use in the Three-River Headwater Region (TRHR) is mainly dominated by natural grassland used for grazing. As for the socioeconomic condition, the rural population accounts for 75%, and free grazing and mobile grazing are the main lifestyles of the local residents [38]. In 2015, the per capita disposable income in the TRHR

was CNY 12,605, only 57.4% of the national average level for that year [39]. Nearly 70% of the population is concentrated in the Yellow River source area, located in the northeastern part of the TRHR [40].

2.2. Data Acquisition and Preprocessing

We first downloaded the daily AVHRR NDVI dataset for the Three-River Headwater Region from 1982 to 2018 from the Big Earth Data Platform for Three Poles [41]. Additionally, we extended the dataset to cover the years 2019 to 2023 by downloading the corresponding AVHRR NDVI data from NASA's LAAD DAAC, which can be accessed at https://ladsweb.modaps.eosdis.nasa.gov/search/order/1/M1_AVH09C1--466 (accessed on 11 June 2024). Both datasets are derived from NOAA's AVHRR products, ensuring continuity and compatibility in the analysis. This dataset was processed to create monthly maximum value composites and denoised using linear interpolation, and areas with no vegetation such as water bodies and snow cover were removed to obtain a monthly resolution NDVI dataset that accurately reflects vegetation growth conditions. Subsequently, we downloaded monthly average precipitation datasets for the Qinghai-Tibetan Plateau (QTP) [35–37], monthly average temperature datasets for China [30–34], annual grazing intensity datasets for the QTP [42], and a 1:1,000,000 vegetation type dataset [11]. Monthly data from January 1984 to December 2015 were selected (except for the grazing intensity dataset, 1984–2015 annually; relatively reliable grazing distribution data beyond 2015 were unavailable, thus restricting our study period), and the vector boundaries of the Three-River Headwater Region [29] were used to clip these datasets, resampling them to a spatial resolution of 0.05 degrees (approximately 5 km) (Table 2). The raster files produced in this step were used for subsequent data analysis.

Table 2. Dataset information and preprocessing methods.

Datasets	Temporal Resolution	Spatial Resolution (Original)	Resample Method
AVHRR NDVI Dataset of TRHR [38]	Day	1/20°	Bilinear
Monthly Average Temperature Dataset of China [30–34]	Month	1/150°	Bilinear
Monthly Average Precipitation Dataset of QTP [35–37]	Month	1/30°	Bilinear
Grazing Intensity Dataset of QTP Grasslands [39]	Year	1/12°	Bilinear
Vegetation Type Dataset of China (Vector) [11]	2001	1:1,000,000	Majority

2.3. Ecosystem Resilience Assessment

To apply the Critical Slowing Down (CSD) method for calculating trends in ecosystem resilience, we first employed the *statsmodels* package in Python 3.8.5 (the same below) for Seasonal and Trend decomposition using Loess (STL) of NDVI time series data spanning 1982 to 2023 (*STL* function, seasonal = 13, trend = 37). This method decomposes time series data with clear seasonal cycles into seasonal, trend, and residual components. The residual components were employed for resilience assessment, thereby eliminating the impacts of seasonal cycles and long-term trends on AR(1) and variance and highlighting short-term productivity fluctuations, consistent with previous studies [23,43]. Next, we used a 60-month sliding window to calculate the local AR(1) and CV (coefficient of variation) of the residual series, obtaining a time series of 445 AR(1) and CV values for each pixel (from June 1984 to June 2021). AR(1) measures the linear correlation between data points in a time series and their immediate predecessors, which can be expressed as follows:

$$X_t = \alpha X_{t-1} + \varepsilon_t, \quad (1)$$

where X_t is the observation at time t, α is the AR(1) regression coefficient, and ε_t is the error term. α can be estimated using the following formula (calculated using the *acf* function in the *statsmodels* package, *tsa* module, Python):

$$\alpha = \frac{\sum_{t=1}^{n-1}\left(X_t - \overline{X}\right)\left(X_{t+1} - \overline{X}\right)}{\sum_{t=1}^{n}\left(X_t - \overline{X}\right)^2} \quad (2)$$

where n is the length of the sliding window, and $\overline{X}$ is the mean of the data within the window. The coefficient of variation (CV) is the ratio of the standard deviation to the mean of the sample, used instead of variance to exclude the impact of the dimension:

$$CV = \frac{S}{\overline{X}} \quad (3)$$

We then calculated the Kendall rank correlation coefficient (τ) between the AR(1) and CV series for each pixel. This metric evaluates the consistency of trends between AR(1) and CV, where -1 indicates opposite trends and 1 indicates completely identical trends, and the formula is as follows:

$$\tau = \frac{2}{n(n-1)}\sum_{i<j}\mathrm{sgn}\left(X_i - X_j\right)\mathrm{sgn}\left(Y_i - Y_j\right) \quad (4)$$

where n is the length of the series being evaluated, X_i and X_j are elements of the first series, Y_i and Y_j are elements of the second series, and sgn is the sign function.

To verify the significance of resilience trend changes over two specific periods, we calculated Kendall's τ for the AR(1) series with time during 1996–2011 and 2012–2021, where 1 represents a consistent increase in AR(1), -1 represents a consistent decrease, and 0 indicates no significant trend. Simultaneously, the *fftpack* module of the Python package *scipy* was utilized to perform phase surrogates on each pixel's AR(1) series over these two periods. This process involves generating phase surrogate sequences by randomly rearranging the phases of the original time series' Fourier transform and then inverting it back [23]. This maintains the overall statistical characteristics of the series, such as variance and means, while disrupting its temporal structure, thereby creating a null model distribution to test the significance of the original series trend. We then used the Wilcoxon signed rank test to examine whether the original series' Kendall τ significantly differed from that of the phase surrogate series. Histograms were also used to depict the distribution of Kendall τ. We also conducted the BFAST (Breaks For Additive Season and Trend) analysis to detect breakpoints in the AR(1) time series where a transition from a decreasing trend to an increasing trend occurs. BFAST analysis decomposes time series data into trend, seasonal, and residual components to identify structural changes; subsequently, we used the Chow test to determine the significance ($p < 0.001$) of the trend differences on either side of the breakpoints. This part of the analysis was conducted using the *bfast* and *strucchange* packages in R 4.4.0, as described in previous studies [43,44].

2.4. Attribution of Resilience

We attempted to determine the factors contributing to the resilience of the Kobresia meadow region from 1996 to 2015 by performing a multivariate linear regression based on ordinary least squares (OLS). This regression analyzed the impacts of average temperature, average precipitation, average productivity (NDVI), and average grazing intensity of each pixel, utilizing the *api* module of the Python *statsmodels* package. The regression model can be expressed as follows:

$$AR(1) = \beta_0 + \beta_1 \times Temp + \beta_2 \times Prcp + \beta_3 \times NDVI + \beta_4 \times Graz + \varepsilon \quad (5)$$

where β_0 is the intercept; β_1, β_2, β_3, and β_4 are the coefficients for the independent variables (temperature (*Temp*), precipitation (*Prcp*), NDVI, and grazing intensity (*Graz*), respectively); and ε is the error term.

Thereafter, the influences of the AR(1) series across regions with varying levels of temperature, precipitation, productivity, and grazing intensity were visualized using a stratified sampling approach. Specifically, the independent variables were categorized into three groups (Table 2), and 100 samples were drawn from each category according to the principle of minimizing the Euclidean distance for the control variables normalized by Z-scores. The clusters centered around the vector of the control variables' mean values. By plotting the average AR(1) series for these samples, the mean and distribution of the control variables within each category were controlled as consistently as possible. The Z-score normalization is expressed by the following formula:

$$Z = \frac{X - \mu}{\sigma} \tag{6}$$

where the variable X represents the original data value, μ is the average of the original data, and σ is the standard deviation of the original data, with Z being the value after standardization. The calculation of the Euclidean distance can be described as follows:

$$d(Z1,\ Z2) = \sqrt{\sum_{i=1}^{n} (z1_i - z2_i)^2} \tag{7}$$

where $Z1$ and $Z2$ are two data points that have been normalized, with n representing the number of control variables, and $z1_i$ and $z2_i$ represent the i^{th} feature (controlled variable value) of $Z1$ and $Z1$, respectively. Subsequently, AR(1) trend line charts were plotted for each level of grazing intensity, temperature, precipitation, and NDVI (vegetation growth condition) to visualize the independent impact of each factor on resilience.

Finally, we conducted an attribution to the temporal dynamics of ecosystem resilience by calculating the Kendall τ for each pixel between AR(1) and each of the following variables respectively: temperature, precipitation, NDVI, and grazing intensity.

3. Results

3.1. Trend of Ecosystem Resilience in the TRHR

First of all, we plotted the average AR(1) trends for each subregion of the TRHR based on the obtained AR(1) time series, with the coefficient of variation (CV) used for validation (Figure 2). The graphs revealed a good match between the two indicators, indicating the reliability of the assessment (Figure 2). Meanwhile, despite some differences in the AR(1) trends across the three regions, there appeared to be a steady decline between 1996 and 2011, corresponding to an increase in ecosystem resilience. Although there was a rebound in the trend after 2012, the average AR(1) distribution graphs before and after the year 2000, when protected areas were established, indicate a general trend of increasing resilience in the Three-River Headwater Region within our study period (Figure 3a,b). To verify the significance of the AR(1) trends from 1996 to 2011 and 2012 to 2021 at the pixel scale, we calculated the Kendall τ of AR(1) over time for each pixel, and the results are presented as raster and histogram charts Figures 3c,d and 4). The images show that the resilience of the ecosystems in all subregions experienced a significant rising trend (AR(1) decreased) between 1996 and 2011 and then significantly decreased (AR(1) increased) from 2012 to 2021, despite some extent of spatial heterogeneity. Specifically, from 1996 to 2011, the Yangtze River Source Region, the Yellow River Source Region, and the Lantsang River Source Region experienced a decrease in AR(1) in 82.7%, 83.9%, and 67.8% of the areas, respectively; in 2012–2021, this proportion dropped to 23.0%, 19.0%, and 10.0%, indicating a rebound in resilience trends. Phase surrogate series were also constructed and Wilcoxon signed rank tests were conducted, and all p-values were far less than 0.001.

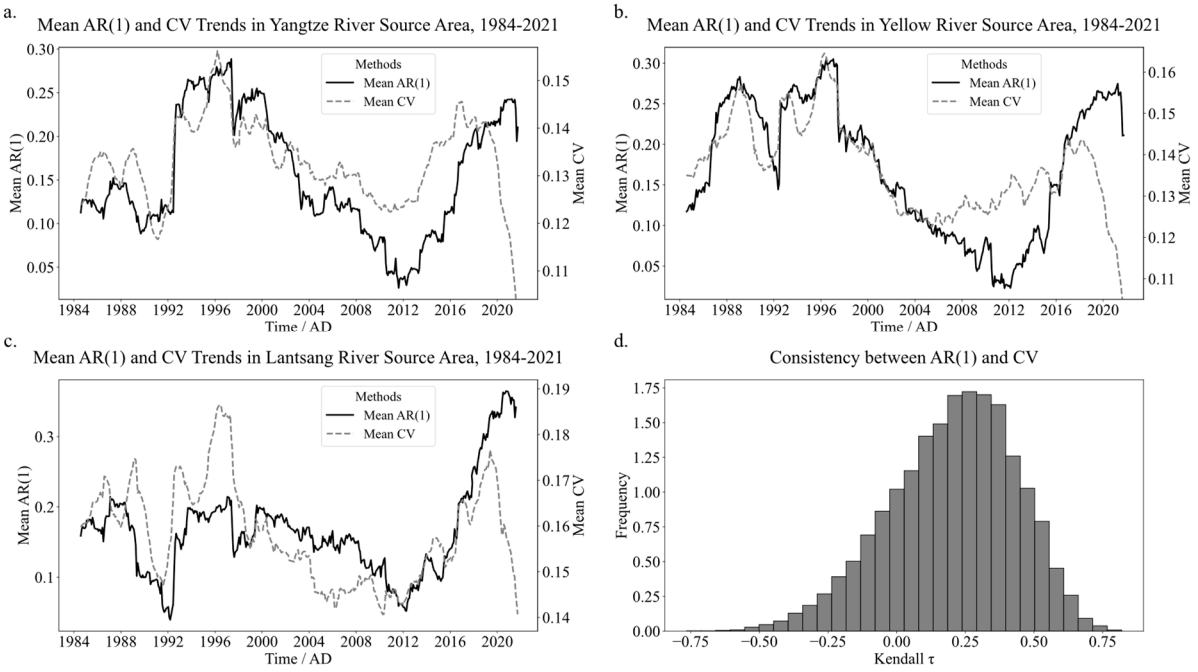

Figure 2. AR(1) trends across the subregions of the TRHR.

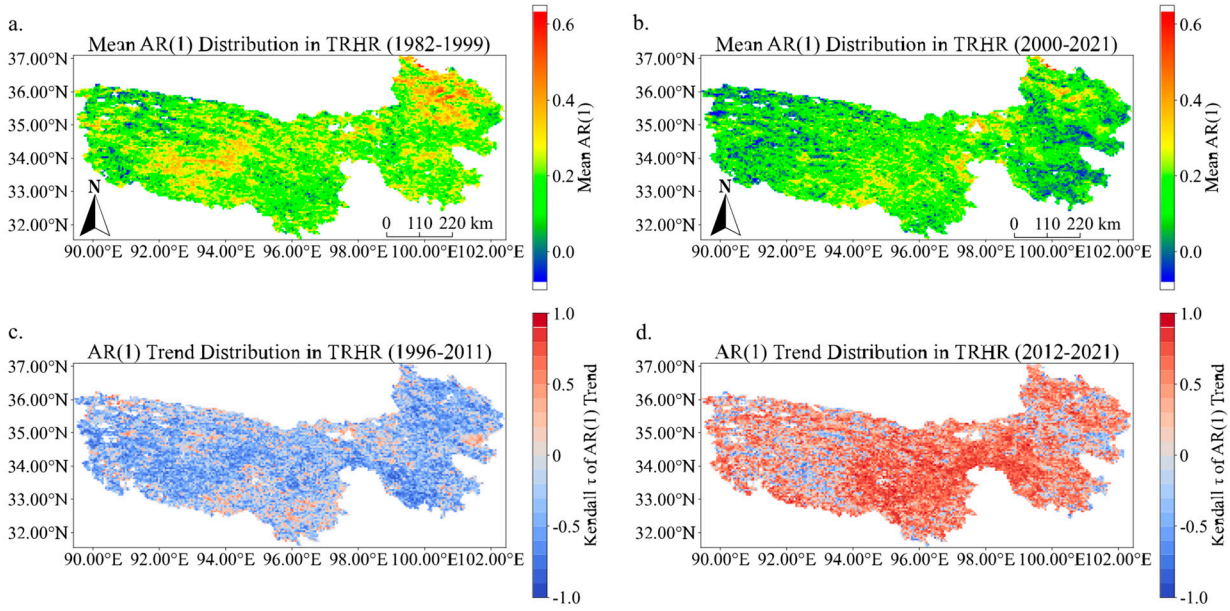

Figure 3. Average AR(1) distribution maps and Kendall τ distribution maps of different periods.

Furthermore, we divided the study area according to vegetation type and plotted the AR(1) time series curves for areas with different types of vegetation (Figure 5). The results indicate that the AR(1) values for different vegetation types generally share the same trend, despite slight differences in absolute values.

The breakpoint identification results indicate that 85.2% of the pixels experienced at least one significant transition from a decreasing to an increasing trend in AR(1) between 1996 and 2021, with 53.7% of these transitions occurring between 2006 and 2011.

In summary, the establishment of the protected area and the grazing restrictions implemented in 2000 have led to an improvement in ecosystem resilience in the TRHR. Additionally, it has been confirmed that around 2011, the TRHR underwent a significant resilience transition affecting the majority of the area and all major vegetation types.

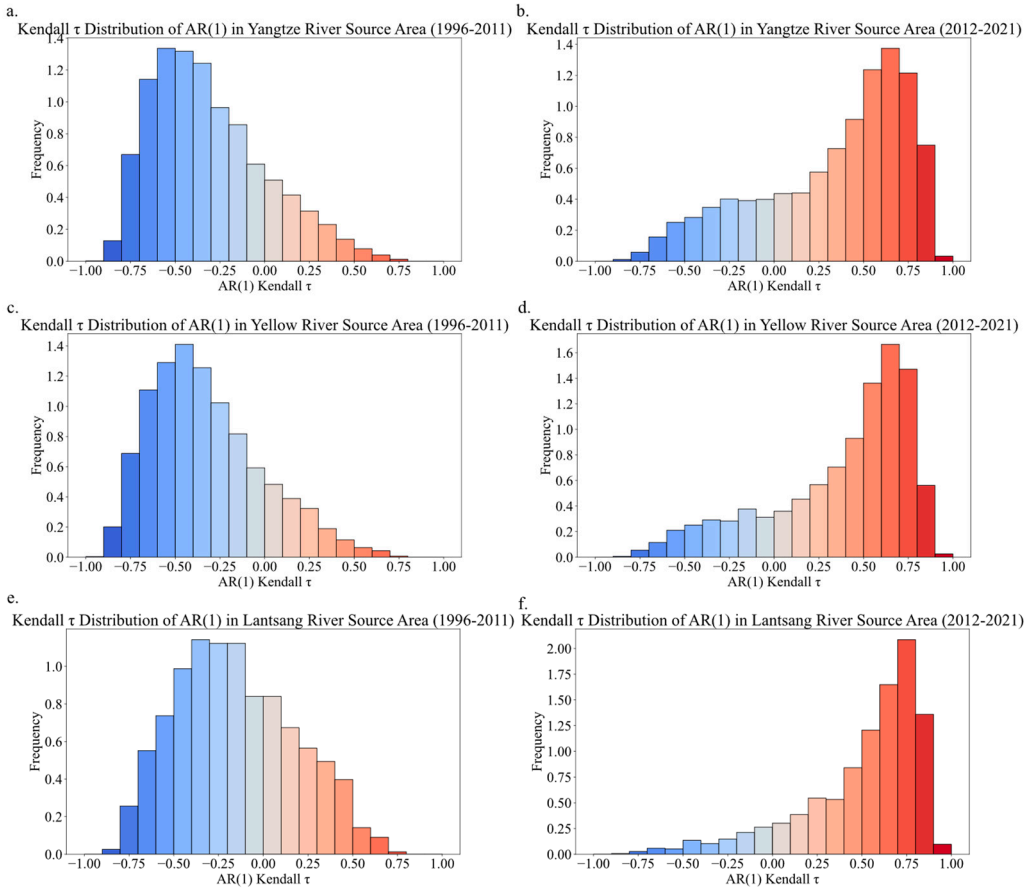

Figure 4. Histograms of AR(1) Kendall τ distribution in subregions from 1996 to 2011 and 2012 to 2021 (The color mapping is consistent with Figure 3c,d.).

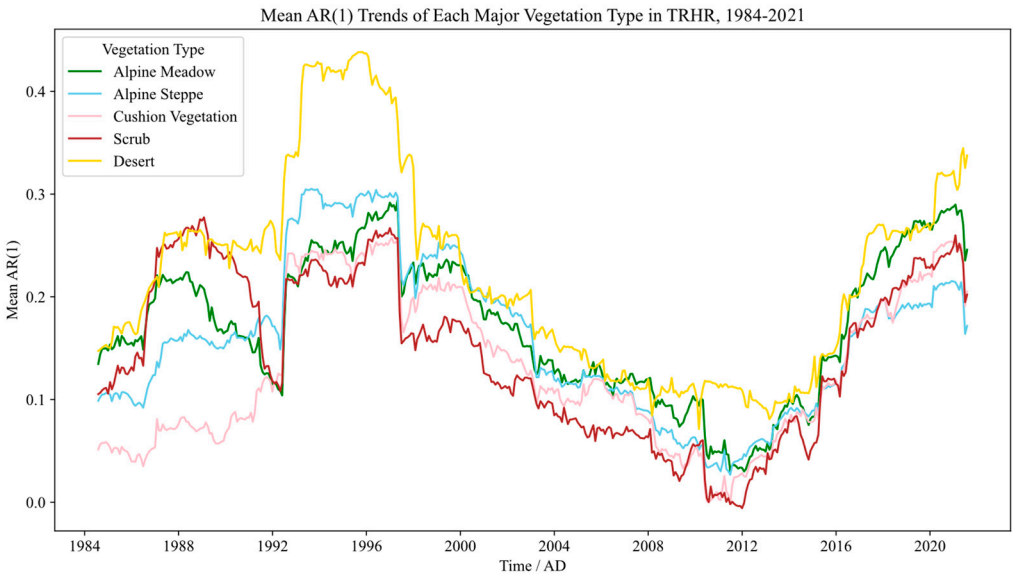

Figure 5. Mean AR(1) trends of each major vegetation type.

3.2. Impact of Average Variable Levels on Resilience

Next, we conducted an attribution analysis of the AR(1) patterns in the Kobresia meadow area (consisting of 4323 pixels). The results of multiple linear regression showed that the average AR(1) of the pixels was significantly correlated with average annual precipitation and NDVI, but not with annual average temperature or grazing intensity

(Table 3). The model explained 10.6% of the variation in AR(1) (R^2 = 0.106). Grouped plots of the levels of independent variables indicated that AR(1) predominantly decreased with increasing precipitation and NDVI, while showing no clear linear relationship with temperature and grazing intensity (Figure 6, Table 4), consistent with the findings of the linear regression analysis.

Table 3. Regression analysis of ecosystem resilience based on temperature, precipitation, vegetation productivity, and grazing intensity.

Variables	Coefficient	Std Err	t-Value	*p*-Value	Confidence Interval (0.95)	VIF
Const	0.2958	0.009	34.245	<0.001	[0.279, 0.313]	--
X1: Mean Temperature	0.0002	6.61×10^{-5}	2.751	0.006	$[5.23 \times 10^{-5}, 0]$	1.993
X2: Mean Precipitation	−0.9019	0.115	−7.871	<0.001	[−1.127, −0.677]	1.480
X3: Mean Grazing Intensity	2.736×10^{-7}	2.04×10^{-7}	1.339	0.181	$[-1.27 \times 10^{-7}, 6.74 \times 10^{-7}]$	1.889
X4: Mean NDVI	−0.3429	0.031	−10.938	<0.001	[−0.404, −0.281]	3.340

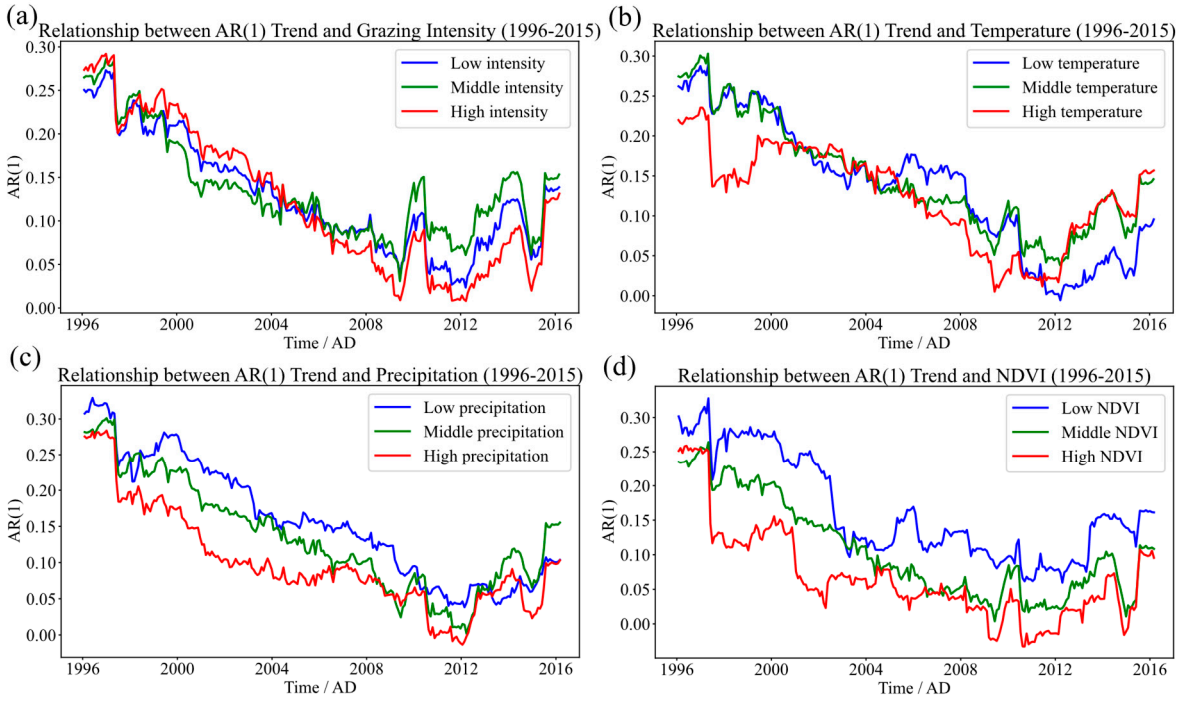

Figure 6. Mean AR(1) trend under different levels of grazing intensity, temperature, precipitation, and vegetation growth condition (NDVI).

Table 4. Categorization of factors by level.

Factors	Low	Middle	High
Mean Temperature (°C)	<0	0–7.5	>7.5
Mean Precipitation (mm/year)	<500	500–800	>800
Mean NDVI	0.1 < 0.25	0.25–0.4	>0.4
Mean Grazing Intensity (SU/(pixel × year))	5000–10,000	10,000–15,000	15,000–20,000

3.3. Impact of Temporal Dynamics of Variables on Resilience

For this section of the analysis, we computed the temporal correlation (Kendall's τ) between AR(1) and temperature, precipitation, NDVI, and grazing intensity for each pixel (Figure 7). The findings reveal that grazing intensity significantly outperforms the other

three variables in explaining the variation in AR(1) trends. Specifically, 60.9% of the areas exhibit a positive Kendall's τ with grazing intensity, and 23.6% of the areas (primarily in the southern part of the Yellow River Source Region) have a Kendall's τ greater than 0.25, whereas the proportions for NDVI, temperature, and precipitation are only 8.2%, 1.9%, and 1.2%, respectively. These results indicate that anthropogenic activities, represented by grazing, are the primary drivers of changes in ecosystem resilience in the TRHR, compared to natural factors.

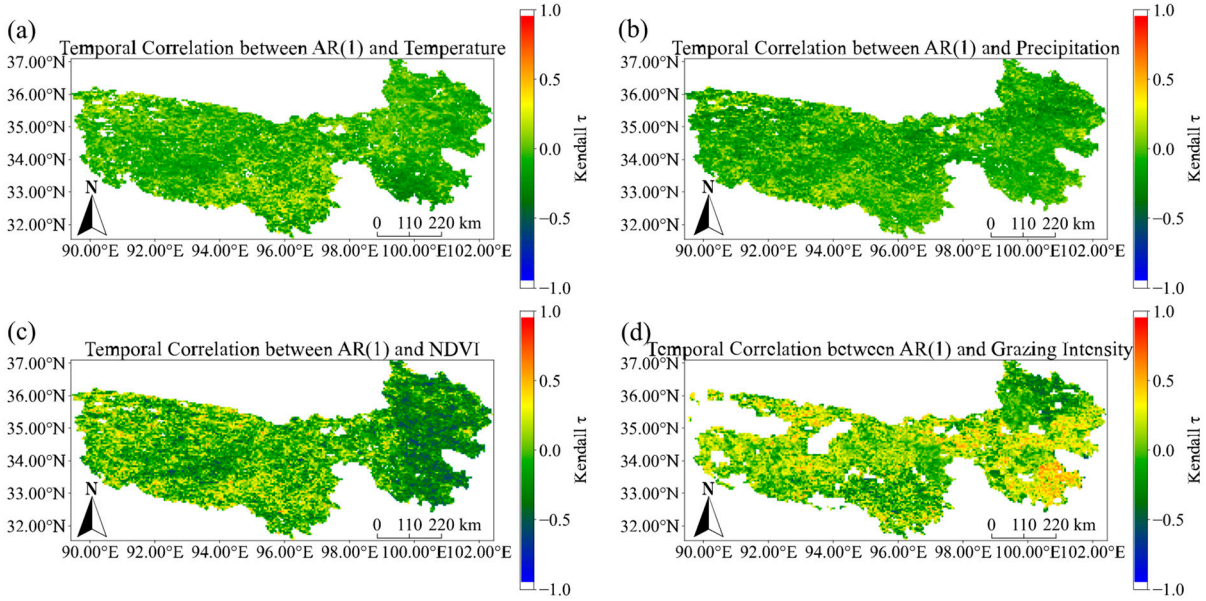

Figure 7. Spatial distribution of temporal correlation between AR(1) and temperature, precipitation, NDVI, and grazing intensity (1984–2015).

4. Discussion

4.1. Reliability of Ecosystem Resilience Assessment

The assessment of ecosystem resilience using the CSD method based on remote sensing NDVI data can be quite sensitive to data noise due to the calculation involving the dynamics of NDVI data over short periods. Taking this into account, although we already denoised the NDVI data, we also calculated both AR(1) and CV, the two indicators of the CSD method, for verification. Theoretically, when random noise occurs in the time data, the CV increases; at the same time, the correlation between data points and their adjacent temporal data points weakens, leading to a decrease in AR(1). However, our results showed that the two indicators shared similar trends, which is contrary to the effects of random noise. Therefore, our assessment of the resilience trend changes is considered to be relatively reliable.

4.2. Spatial Dimension Attribution

Multivariate linear regression analysis of the average levels of NDVI, surface temperature, precipitation, grazing intensity, and AR(1) for each pixel (Kobresia meadows only) from 1996 to 2015 indicated that during this period, when ecosystem resilience experienced continuous increases and decreases, the spatial distribution patterns of precipitation and vegetation growth condition (NDVI) were the primary factors influencing resilience distribution, rather than temperature and grazing intensity. The impact of annual precipitation can be attributed to plant physiological responses; under the same vegetation type, a lower water supply leads to increased water stress in plants, reducing their internal water regulation ability and slowing their response to disturbances [23]. This aligns with findings from other grassland resilience studies [45], particularly in arid and semi-arid areas, where water is a key factor influencing vegetation dynamics [46–48]. The effect of vegetation growth conditions (or productivity) on resilience is complex. Although some studies suggest a

positive correlation, the definitive relationship between productivity and resilience remains under debate [49]. This variability may result from different dominant mechanisms in different ecosystems. However, within our study area, this relationship is significant, suggesting that a higher population density in the Kobresia meadow may provide more propagules and a more stable microenvironment conducive to the establishment of new individuals [50]. Additionally, areas with dense vegetation tend to have higher species diversity and functional redundancy, allowing redundant species to compensate for the loss of functionally similar species when disturbances occur, thereby enhancing ecosystem resilience [51].

4.3. Impact of Grazing Intensity on Resilience

In our analysis, changes in grazing levels were the most effective factor in explaining changes in ecosystem resilience, surpassing the explanatory power of NDVI, temperature, and precipitation, despite the spatial analysis indicating that grazing levels' spatial pattern was not significantly related to ecosystem resilience. This suggests that long-term, stable grazing does not harm ecosystem resilience; rather, continuously increasing grazing intensity may disrupt this balance, leading to a decline in resilience and approaching critical thresholds. The high Kendall τ also indicates that this impact can be reversed with decreased grazing intensity. It is important to note that this relationship varies significantly across different spatial areas. For example, in the northern part of the Yellow River Source Region, resilience is positively correlated with grazing intensity, opposite to the southern region. We speculate that the impact of grazing intensity on grassland resilience is complex and nonlinear. For instance, although grassland degradation is exacerbated and the soil structure is damaged by overgrazing, moderate grazing can promote plant growth and maintain higher species diversity by reducing canopy shading of solar radiation and providing excrement to enhance soil fertility [52,53]. In addition to the direct slowing of grassland recovery due to livestock feeding, grazing activities can significantly alter the community structure of meadows, damaging or maintaining their diversity [54,55]. Different grazing intensities may lead the Kobresia alpine meadow community to several distinct stable states [12,56,57]. As the grazing intensity increases, the total biomass decreases, while the ratio of Kobresia biomass to grass biomass increases [56,57]. Different community compositions will exhibit dissimilar responses to disturbances. Although the mechanisms by which grazing intensity affects grassland resilience require further investigation, we recommend that a seasonal grazing system be prioritized over year-round grazing to reduce the impact of grazing activities on vegetation composition [55], thereby maintaining the relative stability of ecosystem properties and minimizing the likelihood of regime shifts.

4.4. Resilience and Ecosystem Critical Tipping Points

A critical tipping point in an ecosystem refers to the threshold at which the system transitions from one state to another under certain pressures or disturbances. Beyond this point, the ecosystem may undergo rapid and drastic changes. In systems ecology, the approach of an ecosystem to a critical tipping point is often marked by a significant decline in resilience; therefore, AR(1) not only is an indicator of the speed at which an ecosystem recovers from disturbances but also often reflects the system's proximity to regime shifts [22,58]. The dynamics of the annual average NDVI in the Three-River Headwaters Region are plotted in Figure 8, where the blue dashed line represents the regression line of NDVI over the entire study period, with its equation indicated in the top left corner; the positions indicated by the dark blue vertical solid lines represent the two tipping points, dividing the NDVI changes into several significantly different periods, which are marked by the red dashed lines (Figure 8). We can see a significant jump in NDVI around 1996, corresponding to a peak in AR(1); another jump occurred around 2019, with AR(1) reaching nearly the same level as in 1996 (Figure 8). Therefore, in the TRHR region, the rise in AR(1) is likely associated with the system approaching critical points, underscoring the importance of monitoring resilience indicators for the conservation of grassland ecosystems

in this area. Based on the trend of AR(1), the current ecosystem is likely undergoing a critical transition (with our data ending in December 2023). Conducting more detailed community-level analyses based on recent field survey data from the region will help deepen our understanding of the mechanism of this regime shift.

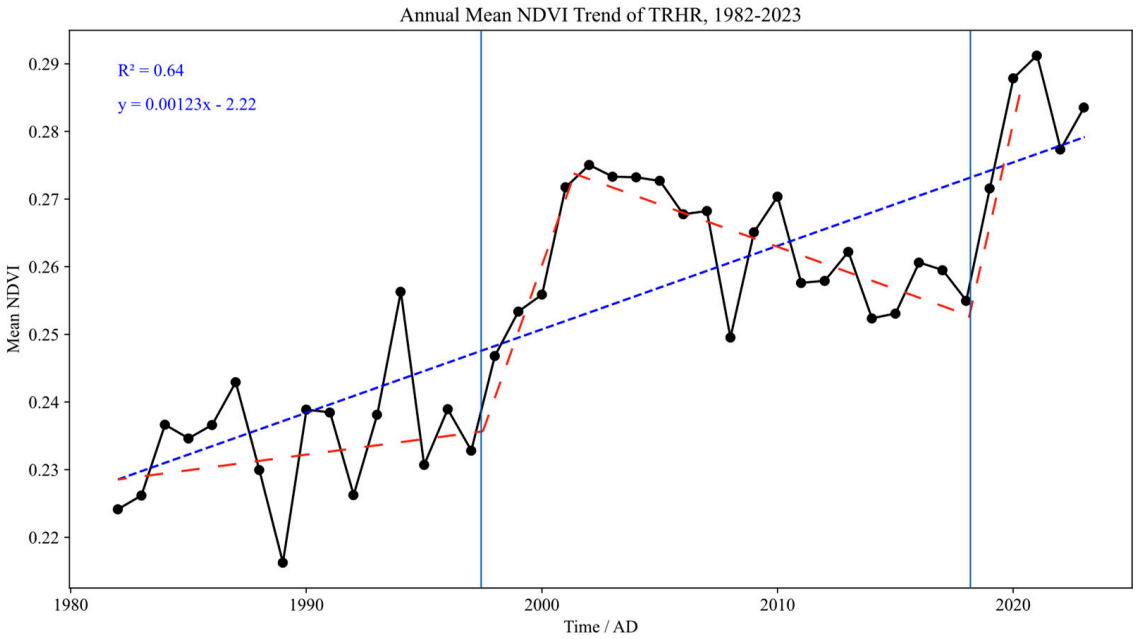

Figure 8. Possible tipping points showed by annual mean NDVI trend of the TRHR.

4.5. Limitations and Challenges

Data preprocessing is not the main focus of this study. Therefore, we adopted a simple interpolation method after monthly maximum value synthesis. Specifically, data points with an NDVI difference exceeding 0.15 from the adjacent months were replaced with their average. We believe this method is sufficient to eliminate obvious outliers while preserving the original fluctuations as much as possible. Indeed, the choice of dataset and filtering method may impact the analysis [59]. In future research, we will consider using better datasets and evaluating the effects of different filtering methods on resilience assessment.

Theoretically, vegetation types have some impact on resilience. However, our findings indicate that for the most part, the resilience trends of different vegetation types were generally similar, although low-productivity vegetation (alpine steppe, cushion vegetation, desert) appeared to differ from alpine meadows and shrubs during the period from 1988 to 1992. Some studies suggest that the vegetation types on the Tibetan Plateau have undergone some changes over the past 40 years [60]. In the future, we may consider using remote sensing and machine learning methods to account for the dynamics of vegetation types to better reveal the relationship between ecosystem resilience and vegetation types.

Ecosystem resilience, as an advanced characteristic of complex adaptive systems [61], is influenced by natural factors and human activities in a nonlinear manner. Therefore, we are concerned that multivariate linear regression and Kendall τ calculations may not fully reveal the reasons behind the spatial and temporal patterns of ecosystem resilience. Few studies effectively determine the factors affecting changes in resilience. For example, Boulton et al. (2022) failed to identify the clear cause for the decline in Amazon rainforest resilience starting in the early 2000s, although they believed climate change played a significant role [23]. Additionally, the attribution results of simple models (such as multivariate linear regression) need to be carefully scrutinized to rule out the possibility of spurious correlations. For instance, Hu et al. (2023) found that after the tipping point, the fertilization effect of CO_2 was most closely related to the rise in AR(1) [43]. However, attributing the increase in AR(1) solely to the continuously rising CO_2 concentration may not be convincing,

and the possibility of spurious correlations needs careful consideration. To better explore the factors influencing ecosystem resilience, more complex statistical models or a focus on specific ecological processes are required.

5. Conclusions

Our study utilized Critical Slowing Down (CSD) indicators to reveal the trends in ecosystem resilience in the Three-River Headwater Region (TRHR), an ecologically significant area, from 1984 to 2021. Compared to the period before the establishment of the nature reserve in 2000, the average ecosystem resilience in the TRHR significantly improved between 2000 and 2021. We observed a significant decreasing trend since the late 1990s in most areas of the TRHR, including all major vegetation types, followed by a notable rebound after 2012.

An analysis of the factors affecting ecosystem resilience indicated that, spatially, grasslands with higher average annual precipitation and greater vegetation cover exhibited higher resilience. Temporally, variations in annual grazing intensity were the primary drivers of resilience changes in the TRHR, particularly in the southern part of the Yellow River Headwater Region, with effects far exceeding those of NDVI, temperature, and precipitation.

Our research highlights the importance of effective ecological management measures, such as establishing protected areas and restricting grazing, in improving ecosystem resilience. Additionally, monitoring resilience helps in understanding the emergence of ecological tipping points. Future research should employ more sophisticated statistical models to analyze the causes of changes in ecosystem resilience and focus on experimental studies of specific ecological processes to better understand the mechanisms underlying resilience changes.

Author Contributions: Conceptualization, Z.W.; methodology, Z.W.; software, Z.W.; validation, Z.W.; formal analysis, Z.W.; investigation, Z.W.; resources, W.H.; data curation, Z.W.; writing—original draft preparation, Z.W.; writing—review and editing, W.H. and X.G.; visualization, Z.W.; supervision, W.H.; project administration, W.H.; funding acquisition, W.H. and X.G. All authors have read and agreed to the published version of the manuscript.

Funding: This research was funded by the National Key R&D Program of China (2022YFB3903304), the National Natural Science Foundation of China (41901351, 42001371), and the Fundamental Research Funds for the Central Universities (2042024fg0010).

Data Availability Statement: The original data presented in the study are openly available as follows: Grazing intensity data are available in FigShare at https://figshare.com/articles/dataset/A_high-Oresolution_gridded_grazing_dataset_of_grassland_ecosystem_on_the_Qinghai_Tibet_Plateau_in_1982_2015/20499723 (accessed on 9 March 2024); NDVI data are available at Level-1 and Atmosphere Archive & Distribution System Distributed Active Archive Center (LAADS DAAC) at https://ladsweb.modaps.eosdis.nasa.gov/ (accessed on 11 June 2024) and the Big Earth Data Platform for Three Poles at https://poles.tpdc.ac.cn/ (accessed on 22 March 2024); temperature, precipitation, vegetation type, and regional boundary data are available at the National Tibetan Plateau Data Center at https://data.tpdc.ac.cn/ (accessed on 18 February 2024, 20 February 2024, 12 March 2024 and 22 February 2024, respectively). The AR(1) time series generated in this experiment, as well as the code used, can be requested from the authors via email for appropriate reasons.

Conflicts of Interest: The authors declare no conflicts of interest, and the funders had no role in the design of the study; in the collection, analyses, or interpretation of data; in the writing of the manuscript; or in the decision to publish the results.

References

1. Zhang, X.; Jin, X. Vegetation Dynamics and Responses to Climate Change and Anthropogenic Activities in the Three-River Headwaters Region, China. *Ecol. Indic.* **2021**, *131*, 108223. [CrossRef]
2. Foggin, J.M. Depopulating the Tibetan Grasslands. *Mt. Res. Dev.* **2008**, *28*, 26–31. [CrossRef]
3. Wang, P.; Lassoie, J.P.; Morreale, S.J.; Dong, S. A Critical Review of Socioeconomic and Natural Factors in Ecological Degradation on the Qinghai-Tibetan Plateau, China. *Rangel. J.* **2015**, *37*, 1–9. [CrossRef]

4. Han, Z.; Song, W.; Deng, X.; Xu, X. Trade-offs and Synergies in Ecosystem Service within the Three-Rivers Headwater Region, China. *Water* **2017**, *9*, 588. [CrossRef]
5. Wang, Z.; Song, K.; Hu, L. China's Largest Scale Ecological Migration in the Three-River Headwater Region. *Ambio* **2010**, *39*, 443–446. [CrossRef] [PubMed]
6. Lowdermilk, W.C. The Role of Vegetation in Erosion Control and Water Conservation. *J. For.* **1934**, *32*, 529–536.
7. Jiang, C.; Zhang, L. Ecosystem Change Assessment in the Three-River Headwater Region, China: Patterns, Causes, and Implications. *Ecol. Eng.* **2016**, *93*, 24–36. [CrossRef]
8. Shen, X.; An, R.; Feng, L.; Ye, N.; Zhu, L.; Li, M. Vegetation Changes in the Three-River Headwaters Region of the Tibetan Plateau of China. *Ecol. Indic.* **2018**, *93*, 804–812. [CrossRef]
9. Harris, R.B. Rangeland Degradation on the Qinghai-Tibetan Plateau: A Review of the Evidence of Its Magnitude and Causes. *J. Arid Environ.* **2010**, *74*, 1–12. [CrossRef]
10. Liu, J.; Xu, X.; Shao, Q. Grassland Degradation in the "Three-River Headwaters" Region, Qinghai Province. *J. Geogr. Sci.* **2008**, *18*, 259–273. [CrossRef]
11. Hou, X. *1:1 Million Vegetation Map of China*; National Tibetan Plateau Data Center: Beijing, China, 2019.
12. Lin, L.; Xu, X.; Cao, G.; Zhang, F.; Li, Y.; Huang, J. Self-stabilizing Maintenance Process in Plant Communities of Alpine Meadows under Different Grazing Intensities. *Grassl. Res.* **2023**, *2*, 140–152. [CrossRef]
13. Ives, A.R. Measuring Resilience in Stochastic Systems. *Ecol. Monogr.* **1995**, *65*, 217–233. [CrossRef]
14. Neubert, M.G.; Caswell, H. Alternatives to Resilience for Measuring the Responses of Ecological Systems to Perturbations. *Ecology* **1997**, *78*, 653–665. [CrossRef]
15. Gunderson, L.H. Ecological Resilience—In Theory and Application. *Annu. Rev. Ecol. Syst.* **2000**, *31*, 425–439. [CrossRef]
16. Oliver, T.H.; Heard, M.S.; Isaac, N.J.; Roy, D.B.; Procter, D.; Eigenbrod, F.; Freckleton, R.; Hector, A.; Orme, C.D.L.; Petchey, O.L. Biodiversity and Resilience of Ecosystem Functions. *Trends Ecol. Evol.* **2015**, *30*, 673–684. [CrossRef] [PubMed]
17. Zhai, X.; Liang, X.; Yan, C.; Xing, X.; Jia, H.; Wei, X.; Feng, K. Vegetation Dynamic Changes and Their Response to Ecological Engineering in the Sanjiangyuan Region of China. *Remote Sens.* **2020**, *12*, 4035. [CrossRef]
18. Huang, W.; Swatantran, A.; Johnson, K.; Duncanson, L.; Tang, H.; O'Neil Dunne, J.; Hurtt, G.; Dubayah, R. Local Discrepancies in Continental Cale Biomass Maps: A Case Study Over Forested and Non-forested Landscapes in Maryland, USA. *Carbon Balance Manag.* **2015**, *10*, 19. [CrossRef]
19. Piao, S.; Fang, J.; Zhou, L.; Tan, K.; Tao, S. Changes in Biomass Carbon Stocks in China's Grasslands between 1982 and 1999. *Glob. Biogeochem. Cycles* **2007**, *21*. [CrossRef]
20. Gaitán, J.J.; Bran, D.; Oliva, G.; Ciari, G.; Nakamatsu, V.; Salomone, J.; Ferrante, D.; Buono, G.; Massara, V.; Humano, G. Evaluating the Performance of Multiple Remote Sensing Indices to Predict the Spatial Variability of Ecosystem Structure and Functioning in Patagonian Steppes. *Ecol. Indic.* **2013**, *34*, 181–191. [CrossRef]
21. Jin, Y.; Yang, X.; Qiu, J.; Li, J.; Gao, T.; Wu, Q.; Zhao, F.; Ma, H.; Yu, H.; Xu, B. Remote Sensing-based Biomass Estimation and its Spatio-temporal Variations in Temperate Grassland, Northern China. *Remote Sens.* **2014**, *6*, 1496–1513. [CrossRef]
22. Dakos, V.; Carpenter, S.R.; van Nes, E.H.; Scheffer, M. Resilience Indicators: Prospects and Limitations for Early Warnings of Regime Shifts. *Philos. Trans. R. Soc. B Biol. Sci.* **2015**, *370*, 20130263. [CrossRef]
23. Boulton, C.A.; Lenton, T.M.; Boers, N. Pronounced Loss of Amazon Rainforest Resilience since the Early 2000s. *Nat. Clim. Chang.* **2022**, *12*, 271–278. [CrossRef]
24. Smith, T.; Dominik, T.; Niklas, B. Empirical Evidence for Recent Global Shifts in Vegetation Resilience. *Nat. Clim. Chang.* **2022**, *12*, 477–484. [CrossRef]
25. Yao, Y.; Liu, Y.; Fu, F.; Song, J.; Wang, Y.; Han, Y.; Wu, T.; Fu, B. Declined Terrestrial Ecosystem Resilience. *Glob. Chang. Biol.* **2024**, *30*, e17291. [CrossRef] [PubMed]
26. Wu, J.; Sun, Z.; Yao, Y.; Liu, Y. Trends of Grassland Resilience under Climate Change and Human Activities on the Mongolian Plateau. *Remote Sens.* **2023**, *15*, 2984. [CrossRef]
27. Zhang, Y.; Zhang, C.; Wang, Z.; Chen, Y.; Gang, C.; An, R.; Li, J. Vegetation Dynamics and Its Driving Forces from Climate Change and Human Activities in the Three-River Source Region, China from 1982 to 2012. *Sci. Total Environ.* **2016**, *563*, 210–220. [CrossRef]
28. Immerzeel, W.W.; Van Beek, L.P.; Bierkens, M.F. Climate Change will Affect the Asian Water Towers. *Science* **2010**, *328*, 1382–1385. [CrossRef]
29. Wei, Y. *The Boundaries of the Source Regions in Sanjiangyuan Region*; National Tibetan Plateau Data Center: Beijing, China, 2018.
30. Peng, S.; Ding, Y.; Wen, Z.; Chen, Y.; Cao, Y.; Ren, J. Spatiotemporal Change and Trend Analysis of Potential Evapotranspiration over the Loess Plateau of China during 2011–2100. *Agric. For. Meteorol.* **2017**, *233*, 183–194. [CrossRef]
31. Peng, S.; Gang, C.; Cao, Y.; Chen, Y. Assessment of Climate Change Trends over the Loess Plateau in China from 1901 to 2100. *Int. J. Climatol.* **2018**, *38*, 2250–2264. [CrossRef]
32. Peng, S. *1-km Monthly Mean Temperature Dataset for China (1901–2022)*; National Tibetan Plateau Data Center: Beijing, China, 2019.

33. Peng, S.; Ding, Y.; Liu, W.; Li, Z. 1 km Monthly Temperature and Precipitation Dataset for China from 1901 to 2017. *Earth Syst. Sci. Data* **2019**, *11*, 1931–1946. [CrossRef]
34. Ding, Y.; Peng, S. Spatiotemporal Trends and Attribution of Drought across China from 1901–2100. *Sustainability* **2020**, *12*, 477. [CrossRef]
35. Zhou, X.; Yang, K.; Ouyang, L.; Wang, Y.; Jiang, Y.; Li, X.; Chen, D.; Prein, A. Added Value of Kilometer-scale Modeling over the Third Pole Region: A CORDEX-CPTP Pilot Study. *Clim. Dyn.* **2021**, *57*, 1673–1687. [CrossRef]
36. Yang, K.; Jiang, Y. *A Long-Term (1979–2020) High-Resolution (1/30) Precipitation Dataset for the Third Polar Region (TPHiPr)*; National Tibetan Plateau Data Center: Beijing, China, 2022.
37. Jiang, Y.; Yang, K.; Qi, Y.; Zhou, X.; He, J.; Lu, H.; Li, X.; Chen, Y.; Li, X.; Zhou, B. TPHiPr: A Long-term (1979–2020) High-Accuracy Precipitation Dataset (1/30°, daily) for the Third Pole Region Based on High-resolution Atmospheric Modeling and Dense Observations. *Earth Syst. Sci. Data* **2023**, *15*, 621–638. [CrossRef]
38. Sheng, W.; Zhen, L.; Xiao, Y.; Hu, Y. Ecological and Socioeconomic Effects of Ecological Restoration in China's Three River Source Region. *Sci. Total Environ.* **2019**, *650*, 2307–2313. [CrossRef] [PubMed]
39. Qinghai Provincial Bureau of Statistics NBS Survey Office in Qinghai. *Qinghai Statistical Yearbook 2016*; China Statistics Press: Beijing, China, 2016.
40. Wang, C.; Wang, J. Kilometer Grid Dataset of China's Historical Population Spatial Distribution (1990–2015). National Tibetan Plateau/Third Pole Environment Data Center 2022. Available online: https://data.tpdc.ac.cn/zh-hans/data/d8c4df4c-eff1-495c-86c0-0ac33f4c57df (accessed on 30 July 2024).
41. Wang, X. Sanjiangyuan AVHRR NDVI Dataset (1981–2020). A Big Earth Data Platform for Three Poles. 2023. Available online: http://poles.tpdc.ac.cn/zh-hans/data/2cd787ea-f98e-48db-87c2-f9e1ced6a01d/ (accessed on 22 March 2024).
42. Meng, N.; Wang, L.; Qi, W.; Dai, X.; Li, Z.; Yang, Y.; Li, R.; Ma, J.; Zheng, H. A High-resolution Gridded Grazing Dataset of Grassland Ecosystem on the Qinghai–Tibet Plateau in 1982–2015. *Sci. Data* **2023**, *10*, 68. [CrossRef] [PubMed]
43. Hu, Y.; Wei, F.; Fu, B.; Wang, S.; Zhang, W.; Zhang, Y. Changes and Influencing Factors of Ecosystem Resilience in China. *Environ. Res. Lett.* **2023**, *18*, 094012. [CrossRef]
44. Verbesselt, J.; Hyndman, R.; Newnham, G.; Culvenor, D. Detecting Trend and Seasonal Changes in Satellite Image Time Series. *Remote Sens. Environ.* **2010**, *114*, 106–115. [CrossRef]
45. Stuart-Haëntjens, E.; De Boeck, H.J.; Lemoine, N.P.; Mänd, P.; Kröel-Dulay, G.; Schmidt, I.K.; Jentsch, A.; Stampfli, A.; Anderegg, W.R.; Bahn, M. Mean Annual Precipitation Predicts Primary Production Resistance and Resilience to Extreme Drought. *Sci. Total Environ.* **2018**, *636*, 360–366. [CrossRef]
46. Huxman, T.E.; Smith, M.D.; Fay, P.A.; Knapp, A.K.; Shaw, M.R.; Loik, M.E.; Smith, S.D.; Tissue, D.T.; Zak, J.C.; Weltzin, J.F. Convergence Across Biomes to a Common Rain-use Efficiency. *Nature* **2004**, *429*, 651–654. [CrossRef]
47. Hua, T.; Wang, X.; Zhang, C.; Lang, L.; Li, H. Responses of Vegetation Activity to Drought in Northern China. *Land Degrad. Dev.* **2017**, *28*, 1913–1921. [CrossRef]
48. Liu, C.; Yan, X.; Jiang, F. Desert Vegetation Responses to the Temporal Distribution Patterns of Precipitation across the Northern Xinjiang, China. *Catena* **2021**, *206*, 105544. [CrossRef]
49. Yan, H.; Zhan, J.; Zhang, T. Resilience of Forest Ecosystems and Its Influencing Factors. *Procedia Environ. Sci.* **2011**, *10*, 2201–2206. [CrossRef]
50. Standish, R.J.; Daws, M.I.; Gove, A.D.; Didham, R.K.; Grigg, A.H.; Koch, J.M.; Hobbs, R.J. Long-term Data Suggest Jarrah-forest Establishment at Restored Mine Sites is Resistant to Climate Variability. *J. Ecol.* **2015**, *103*, 78–89. [CrossRef]
51. Biggs, C.R.; Yeager, L.A.; Bolser, D.G.; Bonsell, C.; Dichiera, A.M.; Hou, Z.; Keyser, S.R.; Khursigara, A.J.; Lu, K.; Muth, A.F. Does Functional Redundancy Affect Ecological Stability and Resilience? A Review and Meta-analysis. *Ecosphere* **2020**, *11*, e03184. [CrossRef]
52. Zhang, Y.; Zhu, J.; Shen, R.; Wang, L. Research Progress on the Effects of Grazing on Grassland Ecosystem. *Chin. J. Plant Ecol.* **2020**, *44*, 553. [CrossRef]
53. Yuan, J.; Li, H.; Yang, Y. The Compensatory Tillering in the Forage Grass Hordeum Brevisubulatum after Simulated Grazing of Different Severity. *Front. Plant Sci.* **2020**, *11*, 792. [CrossRef]
54. Tallowin, J.; Rook, A.; Rutter, S. Impact of Grazing Management on Biodiversity of Grasslands. *Anim. Sci.* **2005**, *81*, 193–198. [CrossRef]
55. Niu, Y.; Yang, S.; Wang, G.; Liu, L.; Hua, L. Effects of Grazing Disturbance on Plant Diversity, Community Structure and Direction of Succession in an Alpine Meadow on Tibet Plateau, China. *Acta Ecol. Sin.* **2018**, *38*, 274–280. [CrossRef]
56. Lin, L.; Cao, G.; Xu, X.; Zhang, F.; Huang, J.; Fan, B.; Li, B.; Li, Y. *Kobresia pygmaea* Meadows as Disclimax Communities in the Same Geographic and Climatic Environments in Qinghai–Tibet Plateau, China. *J. Plant Ecol.* **2023**, *16*, rtad010. [CrossRef]
57. Zhang, C.; Dong, Q.; Chu, H.; Shi, J.; Li, S.; Wang, Y.; Yang, X. Grassland Community Composition Response to Grazing Intensity under Different Grazing Regimes. *Rangel. Ecol. Manag.* **2018**, *71*, 196–204. [CrossRef]
58. Dakos, V.; Kéfi, S. Ecological Resilience: What to Measure and How. *Environ. Res. Lett.* **2022**, *17*, 043003. [CrossRef]
59. Sun, Y.; Peng, D.; Guan, X.; Chu, D.; Ma, Y.; Shen, H. Impacts of the Data Quality of Remote Sensing Vegetation Index on Gross Primary Productivity Estimation. *Remote Sens.* **2023**, *60*, 2275421. [CrossRef]

60. Wang, Y.; Xue, K.; Hu, R.; Ding, B.; Zeng, H.; Li, R.; Xu, B.; Pang, Z.; Song, X.; Li, C. Vegetation Structural Shift Tells Environmental Changes on the Tibetan Plateau over 40 Years. *Sci. Bull.* **2023**, *68*, 1928–1937. [CrossRef]
61. Quinlan, A.E.; Berbés-Blázquez, M.; Haider, L.J.; Peterson, G.D. Measuring and Assessing Resilience: Broadening Understanding Through Multiple Disciplinary Perspectives. *J. Appl. Ecol.* **2016**, *53*, 677–687. [CrossRef]